LIMNOLOGY
and
OCEANOGRAPHY

ASLO

Limnol. Oceanogr. 61, 2016, 806–824

doi: 10.1002/lno.10255

Diversity and productivity of photosynthetic picoeukaryotes in biogeochemically distinct regions of the South East Pacific Ocean

Yoshimi M. Rii,*[1,2] Solange Duhamel,[2,3] Robert R. Bidigare,[2,4] David M. Karl,[1,2] Daniel J. Repeta,[2,5] Matthew J. Church[1,2]

[1]Department of Oceanography, University of Hawai'i at Mānoa, Honolulu, Hawai'i
[2]Daniel K. Inouye Center for Microbial Oceanography: Research and Education, University of Hawai'i at Mānoa, Honolulu, Hawai'i
[3]Lamont-Doherty Earth Observatory, Division of Biology and Paleo Environment, Columbia University, Palisades, New York
[4]Hawai'i Institute of Marine Biology, University of Hawai'i at Mānoa, Kāne'ohe, Hawai'i
[5]Department of Marine Chemistry and Geochemistry, Woods Hole Oceanographic Institution, Woods Hole, Massachusetts

Abstract

Picophytoplankton, including photosynthetic picoeukaryotes (PPE) and unicellular cyanobacteria, are important contributors to plankton biomass and primary productivity. In this study, phytoplankton composition and rates of carbon fixation were examined across a large trophic gradient in the South East Pacific Ocean (SEP) using a suite of approaches: photosynthetic pigments, rates of ^{14}C-primary productivity, and phylogenetic analyses of partial 18S rRNA genes PCR amplified and sequenced from flow cytometrically sorted cells. While phytoplankton >10 μm (diatoms and dinoflagellates) were prevalent in the upwelling region off the Chilean coast, picophytoplankton consistently accounted for 55–92% of the total chlorophyll *a* inventories and >60% of ^{14}C-primary productivity throughout the sampling region. Estimates of rates of ^{14}C-primary productivity derived from flow cytometric sorting of radiolabeled cells revealed that the contributions of PPE and *Prochlorococcus* to euphotic zone depth-integrated picoplankton productivity were nearly equivalent (ranging 36–57%) along the transect, with PPE comprising a larger share of picoplankton productivity than cyanobacteria in the well-lit (>15% surface irradiance) region compared with in the lower regions (1–7% surface irradiance) of the euphotic zone. 18S rRNA gene sequence analyses revealed the taxonomic identities of PPE; e.g., Mamiellophyceae (*Ostreococcus*) were the dominant PPE in the upwelling-influenced waters, while members of the Chrysophyceae, Prymnesiophyceae, Pelagophyceae, and Prasinophyceae Clades VII and IX flourished in the oligotrophic South Pacific Subtropical Gyre. Our results suggest that, despite low numerical abundance in comparison to cyanobacteria, diverse members of PPE are significant contributors to carbon cycling across biogeochemically distinct regions of the SEP.

Primary production in the ocean accounts for nearly half of the net global carbon fixation and a substantial fraction of this productivity occurs in the oligotrophic subtropical gyres (Field et al. 1998; Carr et al. 2006). Picophytoplankton (typically defined as microorganisms <2–3 μm) include unicellular cyanobacteria and photosynthetic picoeukaryotes (PPE) and are significant contributors to productivity and plankton biomass, particularly in the subtropical ocean gyres (Sieburth et al. 1978; Li 1994; Massana 2011). Due to their numerical dominance, *Prochlorococcus* and *Synechococcus* have long been thought to be responsible for a majority of the picophytoplankton productivity in oligotrophic waters. However, several studies have reported that, despite generally low abundances, diverse members of PPE can contribute significantly to biomass and primary production due to their larger cell biovolumes and rapid growth rates (Li 1994; Worden et al. 2004; Jardillier et al. 2010). For example, Worden et al. (2004) estimated that despite small differences in their cell diameters (PPE = ~2.0 μm, *Prochlorococcus* = ~0.7 μm, and *Synechococcus* = ~1.1 μm), PPE carbon content was 6.5-fold to 14-fold greater than that of pico-cyanobacteria. Combined, PPE's larger biovolume and rapid growth rates indicate that PPE can be active and significant components of picophytoplankton population dynamics in the ocean.

*Correspondence: shimi@hawaii.edu

Photosynthetic picoeukaryotes include taxonomically diverse populations, with members scattered widely across many branches of the eukaryotic tree of life (Baldauf 2003; Vaulot et al. 2008; Massana 2011). Studies examining PPE diversity in various regions of the world's oceans show that members of the prasinophyte algae (Mamiellophyceae) have been found to be abundant in nutrient-enriched, coastal regions (Guillou et al. 2004; Romari and Vaulot 2004; Worden 2006), while groups of uncultured prymnesiophytes, chrysophytes, and pelagophytes are often more dominant in open ocean waters (Fuller et al. 2006; Shi et al. 2009; Cuvelier et al. 2010). The cosmopolitan distribution of PPE may reflect their metabolic flexibility. Many PPE taxa appear capable of mixotrophy, combining photosynthetic growth with phagotrophic consumption of other picoplankton for nutrition, thereby complicating characterization of the ecological roles of these organisms (Zubkov and Tarran 2008; Caron et al. 2009; Hartmann et al. 2012). To date, whether or how variability in the composition of picophytoplankton assemblages influences productivity remains unclear. For example, a recent study in the Atlantic Ocean concluded that biomass-specific rates of primary production by PPE appeared largely unaffected by changes in the phylogenetic structure of PPE assemblages (Grob et al. 2011).

In this study, we examined spatial variation in PPE diversity and contributions to productivity across diverse habitats of the South East Pacific Ocean (SEP). This study was conducted as part of the research expedition Biogeochemical Gradients: Role in Arranging Planktonic Assemblages (BiG RAPA), which focused on examining microplankton ecology in the SEP. We sampled biogeochemically distinct regions of the SEP that spanned the productive waters in the permanent upwelling zone off the coast of Chile to the oligotrophic waters of the South Pacific Subtropical Gyre (SPSG). We utilized a suite of approaches to characterize spatial variability in PPE population structure, including photosynthetic pigment-based analyses and assessment of 18S rRNA genes derived from flow cytometrically sorted PPE cells. In addition, we evaluated spatial changes in size-fractionated and PPE group-specific rates of primary productivity. Collectively, we aimed to evaluate the contributions of specific picophytoplankton to plankton biomass and the roles they play in productivity across various nutrient regimes.

Methods

Study site and sample collections

Sampling for this study occurred aboard R/V *Melville* from 18 November (Arica, Chile) to 14 December 2010 (Rapa Nui, Chile). Three main stations were sampled within biogeochemically distinct regions of the SEP: station 1UP in the high productivity, coastal upwelling region; station 7GY in the low productivity, oligotrophic SPSG; and station 4TR in the transitional region between 1UP and 7GY (Fig. 1; Table 1). Additional stations (Stations 2, 3, 5, and 6), located between these main stations, were sampled for a subset of measurements.

A 24-bottle rosette sampler equipped with a Sea-Bird 911+ conductivity, temperature, and depth profiler was used to collect seawater samples. Water samples were collected on specific isopleth surfaces (50%, 25%, 15%, 7%, 3%, 1%, and 0.1% of the sea surface photosynthetically active radiation, or PAR), with additional samples collected at specific biological features, including the depth of the chlorophyll maximum (Chl max). Isopleths were calculated based on vertical profiles of downwelling PAR, measured using a Biospherical Instruments QSP-2300 PAR sensor mounted on the rosette frame. The depths of integration representing the euphotic zone were selected for each station to capture the downwelling light field (down to 0.1% surface PAR), including the Chl max. Thus, the depths of integration used for our calculations were determined to be the depth of the 0.1% surface PAR for stations 1UP-6 and the depth of the Chl max for station 7GY.

Macronutrient analyses

Determination of nitrate plus nitrite ($NO_3^- + NO_2^-$) and phosphate (PO_4^{3-}) in seawater samples were measured on board the R/V *Melville* using a 5-channel, Alpkem and Technicon II™ continuous segmented flow autoanalyzer (Armstrong et al. 1967; Gordon et al. 1994). Detection limits for the instrumental settings used, determined as three times the concentration of our lowest resolvable standard, were 0.16 μM $NO_3^- + NO_2^-$ and 0.011 μM PO_4^{3-}. All nutrient data are available through the Center for Microbial Oceanography: Research and Education (C-MORE) Data System (http://hahana.soest.hawaii.edu/cmoreDS/interface.html).

Photosynthetic pigments

Seawater samples (2 L) were collected for subsequent determination of photosynthetic pigments from eight depths in the euphotic zone (from stations 1UP, 2, 4TR, 5, 6, and 7GY) and vacuum-filtered separately onto 25 mm diameter filters of three pore sizes including glass fiber microfilters (Whatman® GF/F) and 3 μm and 10 μm polycarbonate membrane filters (Millipore Isopore™). Filters were immediately flash-frozen in liquid nitrogen and stored at −80°C until analysis. Pigments were extracted in 100% acetone and analyzed on a Varian 9012 high performance liquid chromatography (HPLC) system (Waters Spherisorb® 5 μm ODS-2 C_{18} column, 200 μL injection) with SpectraSYSTEM Thermo Separation Products dual wavelength UV/VIS UV2000 and fluorescence FL2000 detectors (Bidigare et al. 2005). Pigment identifications were based on absorbance spectra and retention time comparison with a monovinyl chlorophyll *a* (Chl *a*) standard and representative culture extracts. Spectra-Physics WOW® software was used to calculate peak area and a dichromatic equation was used to spectrally resolve mixtures of monovinyl and divinyl Chl *a* (Latasa et al. 1996). Total chlorophyll *a* (TChl *a*) was calculated as the sum of monovinyl Chl *a*, divinyl Chl *a*, and chlorophyllide *a*. The

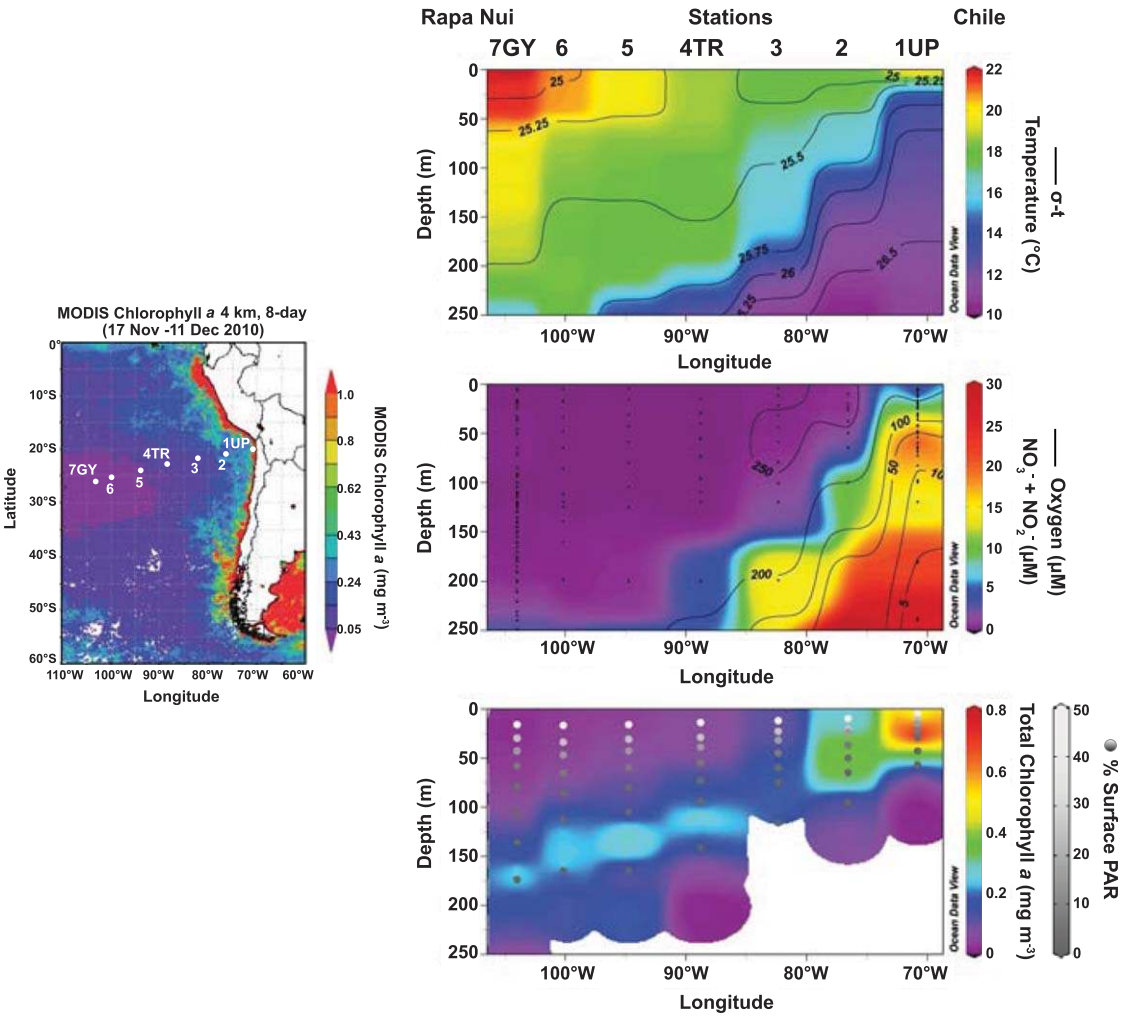

Fig. 1. Contour plots depicting spatial distributions of biogeochemical properties at seven stations along the BiG RAPA transect (produced with Ocean Data View 4.6.2). Left: Map depicting the sampling locations for this study, superimposed on MODIS chlorophyll data obtained from the Giovanni online data system (NASA GES DISC; Acker and Leptoukh 2007); top: Temperature (°C, color) and potential density anomaly (sigma-t; contour lines); center: $NO_3^- + NO_2^-$ (μM, color) and dissolved oxygen (μM, contour lines); bottom: TChl *a* (mg m^{-3}, color) and % surface PAR (white circles darkening in order; 50, 25, 15, 7, 3, 1, 0.1). Black dots indicate depths where samples were collected.

limits of detection were determined as 0.6 ng per injection for chlorophylls and 0.4 ng per injection for carotenoids, which corresponded to an in situ concentration of 0.0045 mg m^{-3} (chlorophylls) and 0.003 mg m^{-3} (carotenoids) for this data set (calculated with 3 mL extract volume and filtered volume of 2 L seawater). Abbreviations and significance of photosynthetic pigments referred to in this study are described in Table 2. All pigment data are available through the C-MORE Data System (http://hahana.soest.hawaii.edu/cmoreDS/interface.html).

Picophytoplankton cell counts

Seawater samples for flow cytometric analyses were collected in 2 mL cryogenic vials containing a final concentration of 0.24% (w/v) paraformaldehyde (PFA, in water, Alfa Aesar 43368). The vials were kept for 15 min in the dark, then flash-frozen in liquid nitrogen and stored at −80°C until analysis. Abundances of PPE, *Prochlorococcus*, and *Synechococcus* were enumerated from PFA-preserved seawater samples based on fluorescence and cell scattering characteristics using a BD Influx™ flow sorter and the data acquisition software Spigot. *Prochlorococcus* cells were enumerated based on forward scatter (FSC) and chlorophyll-based red fluorescence (692 nm center wavelength) signatures using a 488 nm laser, *Synechococcus* cells were identified based on FSC and phycoerythrin-based orange fluorescence (585 nm center wavelength), and PPE cells were defined by their greater FSC, higher red fluorescence, and low orange fluorescence signatures using the data analysis software FlowJo 10.0.7. All flow cytometry cell abundance data are available through the C-MORE Data System (http://hahana.soest.hawaii.edu/cmoreDS/interface.html).

Table 1. Station summary data during the BiG RAPA cruise (18 November–14 December 2010).

	Station ID						
	7GY	**6**	**5**	**4TR**	**3**	**2**	**1UP**
Station location (Lat, Lon)	26.248°S, 103.961°W	25.551°S, 100.136°W	24.560°S, 94.725°W	23.458°S, 88.768°W	22.261°S, 82.348°W	21.178°S, 76.573°W	20.083°S, 70.800°W
Distance from Arica (km)	3637	3249	2695	2078	1407	798	185
$Z_{0.1\%}$ (m)*	137	165	157	141	116	96	57
Chl max (m)	160 ± 13	126 ± 4	123 ± 4	113 ± 7	59 ± 15	40 ± 8	24 ± 3
TChl a_{SFC} (mg Chl m^{-3})†	0.025	0.029	0.041	0.066	0.108	0.207	0.632
TChl a_{EZ} (mg Chl m^{-2})‡	11.6	17.8	20.6	21.8	n/a	26.3	40.0
TChl a >10 μm‡§	0.1 [1%]	0.9 [5%]	0.8 [4%]	0.7 [3%]	n/a	2.0 [8%]	14.6 [37%]
TChl a 3–10 μm‡§	0.8 [7%]	1.2 [7%]	1.0 [5%]	1.9 [9%]	n/a	2.7 [10%]	3.2 [8%]
TChl a < 3 μm‡§	10.7 [92%]	15.8 [88%]	18.8 [91%]	19.2 [88%]	n/a	21.5 [82%]	22.2 [55%]
PPE (x 10^{11} cells m^{-2})‡	1.59 ± 0.05	2.81	1.86	3.30 ± 0.43	6.55	6.76	2.99 ± 1.36
Prochlorococcus (x 10^{11} cells m^{-2})‡	143 ± 10.0	120	142	80.9 ± 13.9	17.4	116	5.24 ± 1.91
Synechococcus (x 10^{11} cells m^{-2})‡	0.77 ± 0.03	0.71	2.07	2.56 ± 0.21	3.45	20.0	19.3 ± 10.6
$NO_3^- + NO_2^-$ (mmol N m^{-2})‡	32.4 ± 30.9	8.07	13.5	17.9 ± 11.0	57.4	248	625 ± 57.0
PO_4^{3-} (mmol P m^{-2})‡	36.7 ± 2.50	39.4	44.9	49.7 ± 0.10	55.3	69.3	100 ± 4.00

*Depth of the 0.1% Surface PAR.
†TChl *a* at surface depth of each station (~5–15 m).
‡Euphotic zone depth-integrated (0.1% surface PAR for St. 1UP-6 and Chl max for St. 7GY).
§(mg Chl m^{-2}), [% sum of TChl *a* size fractions].

Table 2. Euphotic zone depth-integrated* photosynthetic pigment concentrations (mg m^{-2}).

		7GY				4TR				1UP			
Pigment	Dominant pigment in:†	>10 μm	3–10 μm	<3 μm	Total	>10 μm	3–10 μm	<3 μm	Total	>10 μm	3–10 μm	<3 μm	Total
Divinyl Chl *a* (DVChl *a*)	*Prochlorococcus*	0.06	0.24	3.53	3.83	0.02	0.13	6.97	7.12	BLD‡	BLD	0.98	0.98
Zeaxanthin (Zea)	Cyanobacteria	BLD	BLD	5.06	5.06	0.39	0.03	4.86	5.28	0.07	0.12	2.99	3.18
Lutein (Lut)	Chlorophytes	BLD	BLD	BLD	BLD	BLD	BLD	BLD	BLD	0.01	0.03	0.36	0.40
Prasinoxanthin (Pras)	Prasinophytes	BLD	BLD	BLD	BLD	BLD	BLD	BLD	BLD	BLD	0.02	0.35	0.37
19′-hexanoyloxy-fucoxanthin (Hex)	Prymnesiophytes	0.11	0.25	2.37	2.73	0.21	0.90	5.21	6.32	BLD	BLD	6.06	6.06
19′-butanoyloxy-fucoxanthin (But)	Pelagophytes	0.02	0.05	1.32	1.39	0.02	0.20	2.77	2.99	BLD	0.03	1.33	1.36
Fucoxanthin (Fuco)	Diatoms	BLD	BLD	0.55	0.55	BLD	0.08	0.47	0.55	2.19	0.88	2.95	6.02
Alloxanthin (Allo)	Cryptophytes	BLD	BLD	BLD	BLD	BLD	BLD	0.20	0.20	BLD	0.06	0.36	0.42
Peridinin (Peri)	Dinoflagellates	BLD	BLD	0.23	0.22	BLD	0.24	0.21	0.45	9.22	0.31	0.20	9.73

*Euphotic zone depth-integrated (0.1% surface PAR for St. 1UP and 4TR, and Chl max for St. 7GY).
†Pigment descriptions from Jeffrey et al. (2011).
‡BLD: Below the limit of detection (LOD); LOD = 0.0045 mg m^{-3} for chlorophylls, 0.003 mg m^{-3} for carotenoids.

Photosynthetic picoeukaryote cell sorting

Seawater samples were collected, concentrated, and preserved to examine the taxonomic identities of PPE assemblages at the depths of the 50% surface PAR (5 m, 15 m, and 12 m) and the Chl max (48 m, 118 m, and 150 m) of the three main stations (1UP, 4TR, and 7GY, respectively). Seawater samples (2 L) were filtered through in-line 25 mm diameter polycarbonate membranes (pore size 3 μm, Millipore Isopore™), and 2 mL of each pre-filtered sample was collected and preserved in 0.24% (w/v) PFA for subsequent cell enumeration. Pre-filtered seawater was then concentrated to ~50–60 mL (~40-fold) by tangential flow filtration (using Millipore Pellicon® XL 50 Cassette Membranes, Durapore 0.22 μm). During concentration, the inlet pressure of the original water feed was kept constant at 25–30 psig, with the retentate (concentrate) flow at least 2× faster than the permeate flow. The retentate was first backflushed with 10 mL of permeate, then collected in 2 mL and 5 mL cryogenic vials for flow cytometric analyses, containing either 0.24% (w/v) PFA for cell counting, or 7% (v/v) glycerol for sorting and subsequent molecular analyses of PPE cells. All samples were kept for 15 min in the dark, then flash-frozen in liquid nitrogen, and stored at −80°C until analysis.

Cell counts were determined (using the protocol previously described) for samples prior to and after tangential flow concentration to evaluate cell loss deriving from the concentration procedure. For subsequent amplification of the 18S rRNA genes, cell populations were sorted using the BD Influx™ flow sorter from glycerol-preserved samples into 1.5 mL microcentrifuge tubes containing sterile, nuclease-free water totaling up to 10 μL in volume (FSC trigger, 100 μm nozzle tip, 1X BioSure® sheath solution, 1.0 drop purity mode, two tube sort).

Triplicate samples containing 250–1000 PPE cells were collected from the sorting procedure. In addition, the following samples were collected and analyzed as negative controls in the 18S rRNA gene PCR reactions to test for contamination in the flow sorting process: sheath fluid only, 500 1 μm fluorescent microspherical beads (Fluoresbrite, Polysciences), and 250–500 cells of *Prochlorococcus* and *Synechococcus*. All picophytoplankton cells were distinguished using the same FSC and fluorescence-based properties described in the previous section. Tubes containing sorted cells were stored at −80°C until amplification.

Photosynthetic picoeukaryotes sequence analysis

Eukaryote 18S rRNA genes (~1527 bp) were amplified by polymerase chain reaction (PCR) using oligonucleotide primers complementary to regions of conserved sequences close to the respective 5′ and 3′ termini of the 18S rRNA gene (forward: 5′-ACC TGG TTG ATC CTG CCA G-3′ *Escherichia coli* position 7 and reverse: 5′-TGA TCC TTC YGC AGG TTC AC-3′ *E. coli* position 1534; Moon-van der Staay et al. 2000). PCR reaction mixes contained the same reagent concentrations described in Moon-van der Staay et al. (2000) except for 200 nM total deoxyribose nucleoside triphosphates (dNTPs; Life Technologies). Thermal cycling conditions were optimized for direct cell amplification and involved a 15-min hold at 95°C proceeded by 40 cycles at 94°C for 1 min, 55°C annealing for 1 min, and 72°C extension for 1 min, with a final extension at 72°C for 10 min. PCR products were gel-purified (Qiagen MinElute) and cloned into TOPO-TA 4 vectors (Invitrogen). Sequencing was performed using

an Applied Biosystems 3730XL DNA Analyzer using the internal sequencing primer 502f (5′-GGA GGG CAA GTC TGG T-3′) targeting the V4 hypervariable region of the 18S rRNA gene (Worden 2006).

Partial 18S rRNA gene sequences (averaging 680 bp) were checked for chimeras using USEARCH61 (Edgar et al. 2011) and clustered into distinct operational taxonomic units (OTUs) based on the SILVA 119 eukaryote database using similarity thresholds of 97% and 99% (Caporaso et al. 2010; Quast et al. 2013). Clustering at both thresholds yielded equivalent proportions of taxa composition based on class and genus level; for this study, OTUs clustered at 99% are described. Nucleotide sequences were aligned with CLUSTALW (Thompson et al. 1994) and manually inspected and edited. Distance matrices of aligned sequences were generated using CLUSTALW applying the Jukes-Cantor model. The 18S rRNA gene sequences determined in this study have been filed in GenBank under accession numbers KR063739-KR064299.

Rates of ^{14}C-bicarbonate assimilation

Seawater samples for ^{14}C-based primary production measurements were collected from pre-dawn CTD hydrocasts at six depths in the euphotic zone at stations 1UP, 2, 4TR, 6, and 7GY. Duplicate samples from each depth were collected into 75 mL polycarbonate bottles and transferred to a shipboard radiation lab van where samples were inoculated (under subdued light) with a ^{14}C-bicarbonate solution to a final activity of 0.09 MBq mL^{-1}. Bottles were placed in screened bags to simulate in situ light levels and incubated in an on-deck, blue-shielded, surface seawater-cooled Plexiglas container (Arkema 2069, 6.4 mm thickness) for the full photoperiod.

Each bottle was sampled for size-fractionated and cell-specific ^{14}C activities (Duhamel et al. 2006). The total ^{14}C radioactivity added to each bottle was determined by placing 100 μL sample aliquots into 20 mL borosilicate scintillation vials containing 500 μL β-phenylethylamine and 6 mL scintillation cocktail (Perkin Elmer Ultima Gold^{TM} LLT). For size-fractionated ^{14}C activities, 10 mL of inoculated seawater was separately vacuum-filtered onto 25 mm diameter 0.2 μm, 0.6 μm, and 2 μm pore size polycarbonate membranes. Filters were acidified with 150 μL of 1N hydrochloric acid for 24 h, followed by the addition of 6 mL scintillation cocktail. Samples were counted within 6–12 h of the addition of the cocktail in a shipboard Beckman LS6500 liquid scintillation counter for determination of radioactivity. Daily rates of carbon fixation were calculated based on the measured dissolved inorganic carbon concentrations and correcting for isotope fractionation (Steemann Nielsen 1952).

For cell-specific ^{14}C activity measurements, duplicate 5 mL aliquots from the inoculated seawater were preserved in cryovials containing 0.24% (w/v) PFA and stored at −80°C. Cell-specific rates of carbon fixation by PPE, *Prochlorococcus*, and *Synechococcus* were determined by measuring the ^{14}C assimilated into cell populations that had been sorted using a BD Influx^{TM} sorter (FSC trigger, 70 μm nozzle tip, 1X BioSure® sheath solution, 1.0 drop purity mode, two tube sort) into 6.5 mL HDPE scintillation vials (Li 1994; Jardillier et al. 2010; Grob et al. 2011). Each picophytoplankton group was sorted using the same sorting parameters described for molecular analyses, except that an additional laser (457 nm, focused into the 488 nm laser pinhole) was used to improve the detection of dim *Prochlorococcus* cells, particularly in surface samples. Each group was sorted in duplicate ($2.7 \times 10^3 - 20 \times 10^3$ PPE cells, $3.0 \times 10^4 - 20 \times 10^4$ *Prochlorococcus* cells, and $2.0 \times 10^3 - 75 \times 10^3$ *Synechococcus* cells), and linearity between increasing numbers of cells sorted and radioactivity was checked regularly. The radioactivity of the sorted cells was measured following the same procedures as previously described for filtered samples but with 4 mL scintillation cocktail. Resulting radioactivity was normalized to the number of cells sorted (Bq cell^{-1}), and ^{14}C-assimilation rates were converted to mmol C m^{-3} d^{-1} using cell abundance, total added activity, and measured dissolved inorganic carbon concentrations (Moutin et al. 1999; Duhamel and Moutin 2009).

While the samples for the derived 18S rRNA gene sequence information of flow cytometrically sorted PPE populations had been pre-concentrated prior to sorting, samples utilized for the ^{14}C-based rate measurements were not pre-concentrated prior to sorting. However, sort conditions were nearly identical and the fluorescence and scatter characteristics for the picophytoplankton populations did not change for the pre- and post-concentrated samples, supporting the notion that the same groups of organisms were targeted by both approaches.

Hierarchical clustering

Hierarchical clustering based on the Jaccard dissimilarity index (using the "vegan" package in R 3.1.1; Oksanen et al. 2013) was used to compare the relative proportions of photosynthetic pigments (normalized to TChl *a*) and 18S rRNA gene-based assessment of PPE populations at two depths of the three main process stations.

Results

Spatial variability in upper ocean biogeochemistry

The sampling area for this study included diverse hydrographic and biogeochemical regions in the SEP, with strong vertical and longitudinal gradients in upper ocean temperature, nutrient, dissolved oxygen, and TChl *a* concentrations (Fig. 1). Shoaling of isopycnal surfaces due to upwelling along the coast introduced cooler, nutrient-enriched, low oxygen waters to the euphotic zone, with concomitant impacts on phytoplankton biomass, diversity, and productivity. Influences of this upwelling were most evident at the eastern-most stations of the sampling region (stations 1UP

and 2), where euphotic zone (vertically integrated to the 0.1% surface PAR isopleth for stations 1UP to 6, and to the Chl max for station 7GY) inventories of $NO_3^- + NO_2^-$ and PO_4^{3-} ranged 248–625 mmol N m^{-2} and 69–100 mmol P m^{-2} (Table 1). Shoaling of low oxygen waters resulted in suboxic (<10 μM O_2) levels immediately below the subsurface Chl max (~50 m), becoming anoxic at ~100–400 m (Fig. 1). With greater distance offshore, the upper ocean waters became warmer, stratified, and increasingly oligotrophic, with a deepening of this low oxygen waters into the SPSG. The resulting penetration of light through the upper ocean increased westward along the transect, with the 0.1% surface PAR isopleth ranging 57–96 m at stations 1UP and 2, and extending to 165 m into the SPSG (Fig. 1; Table 1). Euphotic zone nutrient inventories decreased into the SPSG, with integrated $NO_3^- + NO_2^-$ concentrations decreasing more than 70-fold from station 1UP to stations 4TR-7GY (Table 1). Euphotic zone inventories of PO_4^{3-} decreased ~2-fold from station 1UP to station 3, then remained relatively consistent at ~37–50 mmol P m^{-2} throughout the oceanic gyre stations (Table 1).

Near-surface ocean TChl *a* concentrations decreased more than an order of magnitude into the oligotrophic waters of the SPSG, with concentrations ranging between 0.2 mg Chl m^{-3} and 0.6 mg Chl m^{-3} at stations 1UP and 2, decreasing to 0.02–0.06 mg Chl m^{-3} at stations 4TR-7GY (Table 1). The resulting euphotic zone inventories of TChl *a* varied by 3.4-fold between stations 1UP and 7GY (40.0 mg m^{-2} and 11.6 mg m^{-2}, respectively; Table 1). The depth of the Chl max also deepened westward, shoaling to ~24 m at station 1UP, and deepening to ~160 m at 7GY (Table 1). The vertical positioning of the Chl max was associated with different isopleth surfaces along the transect, ranging from 7% at station 1UP to 0.1% surface PAR at station 7GY.

Spatial variability in phytoplankton composition

Size-fractionated photosynthetic pigment measurements provided insight into the size distribution of phytoplankton taxa. Consistent with the spatial variability observed in upper ocean biogeochemistry, the size structure, composition, and abundance of phytoplankton varied markedly between the sampling regions. Euphotic zone inventories of size-fractionated TChl *a* revealed that >10 μm cells comprised 37% of TChl *a* at station 1UP and ≤8% of TChl *a* at other stations sampled (Table 1). Picophytoplankton (cells <3 μm) accounted for 55% of the euphotic zone TChl *a* inventories at station 1UP and 82–92% at other stations (Table 1). Contributions by the 3–10 μm size fraction were consistent and relatively low (5–10%) at all stations sampled, with most of the variability in phytoplankton TChl *a* attributable to spatial changes in the >10 μm and picophytoplankton fractions of TChl *a*. Profiles of size-fractionated TChl *a* also indicated vertical variability associated with phytoplankton size structure among the sampling stations. At station 1UP, the picophytoplankton size fraction was dominant in the upper euphotic zone (<40 m; above the 1% surface PAR) and the >10 μm fraction dominated in the lower euphotic zone (~40–59 m; near the 0.1% surface PAR; Fig. 2). At all other stations, the pico-size fraction dominated in the Chl max (Fig. 2).

Hierarchical clustering analyses (based on presence-absence and dissimilarity using the Jaccard index) of TChl *a*-normalized photosynthetic pigments revealed large differences between the phytoplankton sampled at station 1UP, especially in the larger size fraction, compared with other stations (Fig. 3). For example, absolute concentrations of peridinin and fucoxanthin were elevated at 1UP (9.7 mg m^{-2} and 6.0 mg m^{-2}, respectively), particularly in the >10 μm fraction, indicating a greater presence of dinoflagellates and diatoms in the upwelled water (Table 2; Fig. 3). Pigment to TChl *a* ratios for photosynthetic pigments diagnostic of prymnesiophytes (19′-hexanoyloxyfucoxanthin) and pelagophytes (19′-butanoyloxyfucoxanthin) remained relatively consistent across the cruise-track, with a majority of these pigments observed in the picophytoplankton size fraction (Fig. 3). Phytoplankton types were partitioned among the picophytoplankton and the larger size fraction, as indicated by the clustering together of photosynthetic pigments in the picophytoplankton size fractions, separately from pigments measured in the >3 μm fractions (Fig. 3). Concentrations of prasinoxanthin and lutein, pigment biomarkers indicative of the presence of prasinophytes and chlorophytes, respectively, were below the limit of detection at all stations except 1UP (Table 2). Concentrations of alloxanthin, a biomarker diagnostic of cryptophytes, were detectable only at stations 1UP and 4TR. Concentrations of divinyl Chl *a*, a pigment diagnostic of *Prochlorococcus*, were highest at the oceanic stations 4TR and 7GY but in relatively low concentration at station 1UP. However, concentrations of zeaxanthin, an accessory pigment found in all cyanobacteria, were elevated and relatively stable across the transect, including station 1UP (Table 2; Fig. 3).

Flow cytometric quantification of PPE, *Prochlorococcus*, and *Synechococcus* demonstrated spatial changes in picophytoplankton abundance across the sampling transect. Euphotic zone inventories of *Prochlorococcus* were low at station 1UP (5.24×10^{11} cells m^{-2}), becoming increasingly abundant into the SPSG ($17.4–143 \times 10^{11}$ cells m^{-2} at stations 2-7GY; Table 1). Abundances of *Synechococcus* revealed an opposite trend, with abundances greatest in the upwelling region (abundances at stations 1UP and 2 ranged $19.3–20 \times 10^{11}$ cells m^{-2}), and nearly 50-fold lower ($0.71–3.45 \times 10^{11}$ cells m^{-2}) into the SPSG. In contrast, euphotic zone abundances of PPE were much less variable than that of cyanobacteria, ranging ~6-fold over the transect ($1.5–6.8 \times 10^{11}$cells m^{-2}; Table 1), with PPE abundances peaking at stations 2 and 3.

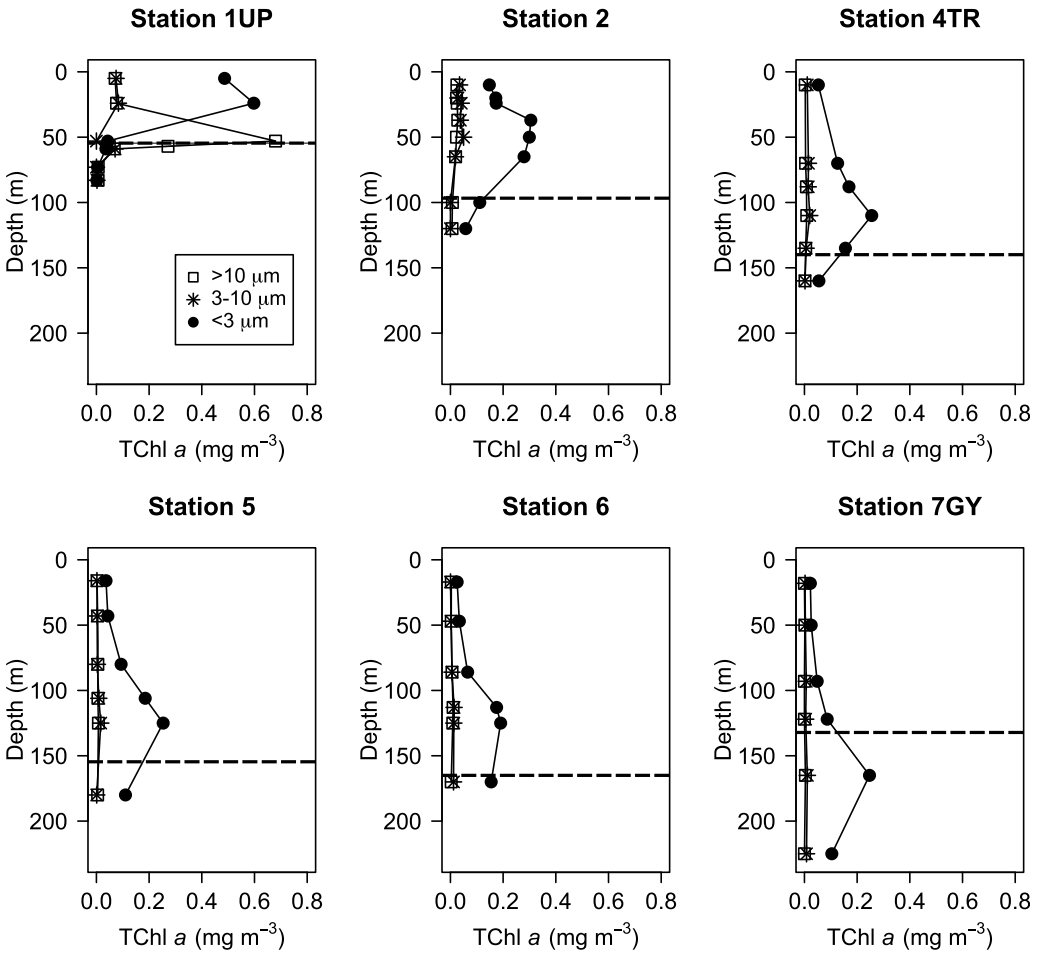

Fig. 2. Depth profiles of size-fractionated TChl *a* concentrations (mg m^{-3}) at stations 1UP, 2, 4TR, 5, 6, and 7GY. Dashed horizontal lines indicate depths of the 0.1% surface PAR.

Composition of PPE assemblages

We amplified and sequenced partial 18S rRNA genes from flow cytometrically sorted PPE populations from the near-surface (50% surface PAR) and the Chl max at stations 1UP, 4TR, and 7GY to examine changes in taxonomic composition. We employed this method of combining molecular analyses with flow-sorted cells to specifically target PPE, as 18S rRNA gene sequences retrieved from filtered seawater samples are often dominated by non-photosynthetic (presumably heterotrophic) picoeukaryotes. No amplification was observed in the control reactions (containing sheath fluid, sorted beads, or sorted cyanobacteria cells). A total of 561 sequences were obtained from flow-sorted PPE assemblages, and sequences were clustered at a 99% sequence similarity threshold into 32 OTUs. Six of these OTU clusters (totaling 35 sequences) derived from taxa not known to be photosynthetic: 2 Ciliophora OTUs (consisting of 21 sequences closely related to ciliates Cryptocaryon JX188358 and Scuticociliatia AY665059), 3 Fungi OTUs (10 sequences affiliated with the genus Malassezia FJ000217, FJ000238, KC673661), and 1 Rhizaria OTU (4 sequences clustering among the Acantharea Group I GU821070). Given our interests in PPE, we removed these sequences from subsequent analyses in this study. Of the remaining 26 OTUs (526 sequences in total), 8 distinct OTUs (108 sequences total) clustered among the Haptophyta, 8 OTUs (280 sequences total) among the Chlorophyta, 5 OTUs (121 sequences total) with the Stramenopiles, 2 OTUs (2 sequences total) with the Cryptophyta, and 3 OTUs (15 sequences total) with the Alveolata (Table 3).

The dominant PPE taxa derived from these flow-sorted cell 18S rRNA gene amplifications differed spatially between the three stations and vertically between the near-surface waters and at the Chl max. Hierarchical clustering analyses (based on the Jaccard index) of the 18S rRNA gene sequences revealed that the PPE assemblages at station 1UP clustered separately from those at 4TR and 7GY (Fig. 4). A large proportion (74–95%) of the sequences retrieved from station 1UP in both near-surface waters and the Chl max were closely related (99.7% sequence identity) to *Ostreococcus* (Mamiellophyceae),

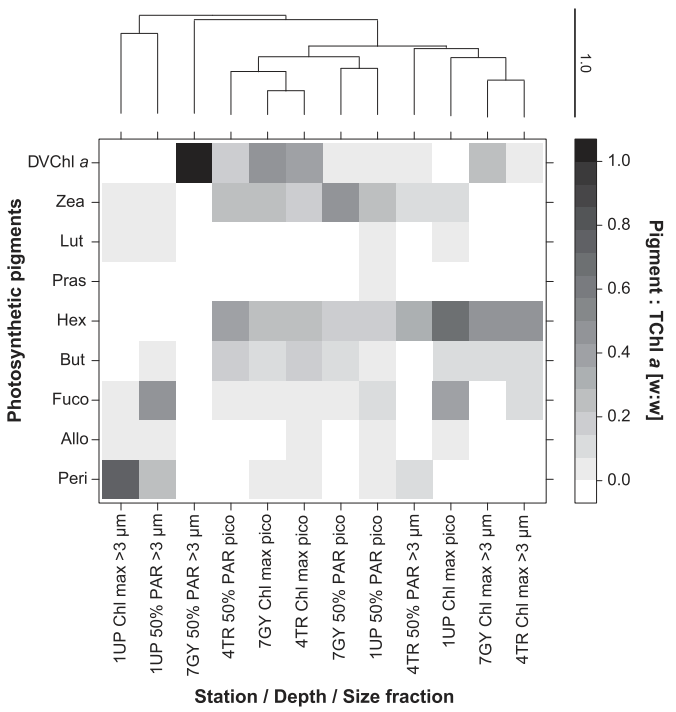

Fig. 3. Horizontal and vertical distributions of photosynthetic pigments (as a ratio to TChl *a*) measured at stations 1UP, 4TR, and 7GY. Relative pigments are binned by station, depth (50% surface PAR isopleth or the Chl max), and size fraction (>3 μm or pico = <3 μm). The dendrogram, at height 1.0 being the most dissimilar, depicts clustering based on the Jaccard index.

which were not detected at any of the other stations sampled (Table 3). In addition, ~15% of sequences from the near-surface and ~2% from the Chl max sequences from station 1UP clustered among haptophytes belonging to the genus *Chrysochromulina*. These *Chrysochromulina* sequences formed two clusters that differed by >97.8% sequence identity, one of which was closely related to *Chrysochromulina simplex*. Other sequences retrieved at station 1UP clustered (>97% sequence identity) among chlorophytes *Nannochloris* and *Micromonas* (~5% and 3% of the sequences from the near-surface water sample, respectively) and cryptophytes *Teleaulax* (~2% of the sequences from the near-surface water sample). In the Chl max, the assemblage included sequences closely related (99.5% sequence identity) to the pelagophyte *Pelagomonas calceolata* (~3% of the sequences from this sample; Table 3).

Photosynthetic picoeukaryote assemblages at both depths at station 4TR clustered together (along with assemblages at the Chl max at station 7GY) according to the Jaccard index, although the dominant sequence-types found at each depth differed (Fig. 4). Sequences closely related (>99% sequence identity) to *Pelagomonas calceolata* and Prasinophyceae clade VII subclade B were retrieved from both depths, but sequences most similar to *Pelagomonas calceolata* comprised 62% of the sequences in the near-surface sample, while the Prasinophyceae clade VII subclade B comprised 52% of the Chl max sequences (Table 3). The assemblage at the Chl max was composed of a greater number of distinct OTUs than the surface assemblage, with a mixture of sequences clustering among Prasinophyceae, Prymnesiophyceae, and Pelagophyceae (Table 3). In addition, 24% of the sequences retrieved from the Chl max at station 4TR grouped among the Alveolata, including those closely related (>98% sequence identity) to Syndiniales Group V, an uncultivated group of presumed parasitic marine alveolates.

We observed a greater number of total distinct OTUs in the oligotrophic SPSG station 7GY than at other stations. The near-surface phytoplankton assemblage clustered separately from the assemblage at the Chl max (Fig. 4), with the near-surface assemblage including Prasinophyceae (four OTU totaling ~63% of sequences; >97% identity) and Chrysophyceae (~31% of total sequences; 99.6% identity;), with small contributions from the haptophyte *Chrysochromulina* and dictyochophyte *Pedinella* (Fig. 4; Table 3). The PPE sequences from the Chl max were dominated (70% of sequences from this depth) by diverse groups of prymnesiophytes (four distinct OTUs) that included sequences closely related (>98% sequence identity) to *Phaeocystis globosa*, *Helicosphaera*, *Chrysochromulina*, and *Imantonia* (Fig. 4; Table 3).

Rates of total and group-specific primary production

Euphotic zone rates of ^{14}C-bicarbonate assimilation varied ~6-fold across the sampling region, with elevated rates (128–137 mmol C m^{-2} d^{-1}) observed at stations 1UP and 2 and rates decreasing to 18–23 mmol C m^{-2} d^{-1} at stations 6 and 7GY in the oligotrophic SPSG (Fig. 5a). Despite large differences in rates of ^{14}C-based primary production between stations, the picophytoplankton size fraction (0.2–0.6 and 0.6–2 μm, combined) consistently accounted for 61–73% of the total (>0.2 μm) ^{14}C-based productivity (Fig. 5b). Rates of ^{14}C-bicarbonate assimilation by the >2 μm size fraction accounted for the remaining 27–38% of the depth-integrated productivity (Fig. 5b).

Group- and cell-specific contributions of PPE, *Prochlorococcus*, and *Synechococcus* to rates of primary productivity were examined based on flow cytometric sorting of ^{14}C-radiolabeled cells at stations 2, 4TR, 6, and 7GY. Rates of ^{14}C-based primary production by PPE and *Prochlorococcus* were approximately equivalent to each other throughout the sampling region, while rates of production by *Synechococcus* were consistently 2-fold to 6-fold lower than either rates of PPE or *Prochlorococcus* production (Table 4). The resulting cell-specific rates of ^{14}C-based primary production by PPE (~16–34 fmol C cell^{-1} d^{-1}) were considerably greater than the rates by *Prochlorococcus* (~0.3–2 fmol C cell^{-1} d^{-1}) or *Synechococcus* (~5–11 fmol C cell^{-1} d^{-1}; Table 4). In total, cumulative rates of primary production by sorted picophytoplankton cells (sum of group-specific rates of primary productivity by PPE, *Prochlorococcus*, and *Synechococcus*)

Table 3. Distribution of 18S rRNA gene clones of PPE as percent of total number of sequences* recovered from each station/depth.

Phylum	Class	Genus (Species)	Accession No. (% Identity)	Sta. 7GY Chl max	Sta. 7GY 50% PAR	Sta. 4TR Chl max	Sta. 4TR 50% PAR	Sta. 1UP Chl max	Sta. 1UP 50% PAR	Reference
Chlorophyta	Mamiellophyceae	*Ostreococcus*	KC583118 (99.7%)	–†	–	–	–	95.2%	74.1%	Red Sea, 10 m; Acosta et al. (2013)
Chlorophyta	Mamiellophyceae	*Micromonas*	GQ863805 (99.3%)	–	–	–	–	–	2.5%	Atlantic Meridional Transect, 10 m; Kirkham et al. (2011)
Chlorophyta	Trebouxiophyceae	*Nannochloris*	AY256258 (99.3%)	–	–	–	–	–	4.9%	Permanently anoxic deep sea basin; Stoeck et al. (2003)
Chlorophyta	Prasinophyceae	Clade IX	FJ537345 (99.1%)	–	5.6%	–	–	–	–	BIOSOPE T65.111, STB12, 40 m; Shi et al. (2009)
Chlorophyta	Prasinophyceae	Clade IX	KF031641 (99.2%)	–	31.5%	1.7%	–	–	–	South China Sea, surface; Wu et al. (2014)
Chlorophyta	Prasinophyceae	Clade IX	JX291959 (97.6%)	–	7.9%	1.7%	–	–	–	North Pacific Ocean; Thompson et al. (2012)
Chlorophyta	Prasinophyceae	Clade VII Subclade A	U40921 (99.5%)	–	18.0%	–	–	–	–	CCMP1205; Potter et al. (1997)
Chlorophyta	Prasinophyceae	Clade VII Subclade B	FJ537357 (99.2%)	–	–	51.7%	7.1%	–	–	BIOSOPE, Oligo station, 150 m; Shi et al. (2009)
Haptophyta	Prymnesiophyceae	*Chrysochromulina*	FJ000253 (97.9%)	–	–	–	–	1.6%	3.7%	Discovery Basin, Mediterranean; Edgcomb et al. (unpubl.)
Haptophyta	Prymnesiophyceae	*Chrysochromulina*	JF698758 (98.9%)	–	–	–	–	–	11.1%	Beaufort Sea, 3 m; Balzano et al. (2012)
Haptophyta	Prymnesiophyceae	*Chrysochromulina*	HM581603 (99.1%)	–	2.2%	–	–	–	–	Subtropical North Atlantic, 75 m; Cuvelier et al. (2010)
Haptophyta	Prymnesiophyceae	*Chrysochromulina*	FJ537355 (98.8%)	5.7%	–	–	–	–	–	BIOSOPE T84.038, STB14, 5 m; Shi et al. (2009)

TABLE 3. Continued

Phylum	Class	Genus (Species)	Accession No. (% Identity)	Sta. 7GY Chl max	Sta. 7GY 50% PAR	Sta. 4TR Chl max	Sta. 4TR 50% PAR	Sta. 1UP Chl max	Sta. 1UP 50% PAR	Reference
Haptophyta	Prymnesiophyceae	Prymnesiales OLI16029	JX291794 (98.6%)	–	–	–	30.6%	–	–	Open ocean, Thompson et al. (2012)
Haptophyta	Prymnesiophyceae	*Phaeocystis* (*globosa*)	JX660986 (99.7%)	18.4%	–	–	–	–	–	Atlantic Ocean; Decelle et al. (2012)
Haptophyta	Prymnesiophyceae	*Imantonia*	AJ402351 (98.3%)	3.4%	–	–	–	–	–	Equatorial Pacific Ocean; Moon-van der Staay et al. (2000)
Haptophyta	Prymnesiophyceae	*Helicosphaera*	FJ537311 (99%)	42.5%	–	8.6%	–	–	–	BIOSOPE T33.008, STB6, 180 m; Shi et al. (2009)
Stramenopiles	Chrysophyceae	Marine chrysophyte	AY046864 (99.6%)	–	31.5%	–	–	–	–	Guaymas Basin hydrothermal vent; Edgcomb et al. (2002)
Stramenopiles	Dictyochophyceae	*Pedinella*	JX291705 (99.6%)	–	2.2%	–	–	–	–	North Pacific Ocean; Thompson et al. (2012)
Stramenopiles	Ochrophyta	MOCH-2	GQ382461 (99.8%)	1.1%	–	3.4%	–	–	–	NW Pacific; Caron et al. (2009) and Massana et al. (2014)
Stramenopiles	Pelagophyceae	*Pelagomonas* (*calceolata*)	U14389 (99.5%)	28.7%	–	8.6%	62.4%	3.2%	–	CCMP1214; Andersen et al. (1993)
Stramenopiles	Labyrinthulomycetes	Marine stramenopile	GU824965 (97.8%)	–	1.1%	–	–	–	–	Micro-oxic water, Cariaco Basin; Edgcomb et al. (2011)
Cryptophyta	Cryptophyceae	*Teleaulax* (*minuta*)	JQ966996 (99.3%)	–	–	–	–	–	1.2%	Cr8EHU, estuarine, Spain; Laza-Martinez et al. (2012)
Cryptophyta	Cryptophyceae	*Teleaulax*	HQ865081 (97.5%)	–	–	–	–	–	1.2%	Saanich Inlet, 10 m; Orsi et al. (2012)

TABLE 3. Continued

Phylum	Class	Genus (Species)	Accession No. (% Identity)	Sta. 7GY Chl max	Sta. 7GY 50% PAR	Sta. 4TR Chl max	Sta. 4TR 50% PAR	Sta. 1UP Chl max	Sta. 1UP 50% PAR	Reference
Alveolata	Dinophyceae	Uncultured dinoflagellate	KC488419 (98.6%)	–	–	1.7%	–	–	–	Atlantic Ocean, station BBL6, 3 m; Dasilva et al. (unpubl.)
Alveolata	Syndiniales	*Amoebophrya*	AY129038 (97.9%)	–	–	–	–	–	1.2%	Coastal Pacific Ocean; Worden (2006)
Alveolata	Syndiniales	Group V	EU793265 (99.3%)	–	–	22.4%	–	–	–	Mediterranean, PROSOPE, 25 m; Guillou et al. (2008)
		Total # of PPE sequences:		100% 87	100% 89	100% 58	100% 85	100% 126	100% 81	

*Total excludes sequences of non-photosynthetic taxa.
†– denotes 0%.

accounted for 63–111% of the measured picoplankton (0.2–2 μm) primary productivity, and 42–70% of total (> 0.2 μm) primary productivity measured on filters (Table 4).

There was also vertical variability in picoplankton contributions to rates of ^{14}C-primary production. At the upwelling-influenced station 2, productivity by PPE and cyanobacteria were comparable in the well-lit waters above 15% surface PAR, with contributions by cyanobacteria increasing in the lower euphotic zone (<7% surface PAR isopleth; Fig. 6). Along the western end of the sampling transect (stations 4TR, 6, and 7GY), PPE contribution to production was greatest in the well-lit upper ocean (>15% surface PAR), with contributions by *Prochlorococcus* increasing deeper in the euphotic zone (<7% surface PAR isopleth; Fig. 6).

Discussion

We identified vertically and longitudinally distinct patterns in picophytoplankton biomass, productivity, and taxonomic diversity across widely differing trophic states in the SEP using a combination of approaches that included size-fractionated photosynthetic pigments and rates of ^{14}C-productivity, flow cytometric sorting of ^{14}C-radiolabeled picoplankton cells, and 18S rRNA gene amplification and sequencing of sorted PPE cells. The upwelling-influenced waters supported a phytoplankton standing stock that consisted of both large (>3 μm) and pico-sized phytoplankton, with approximately equal contributions (45% and 55%, respectively) by both size classes to TChl *a* inventories. In comparison, in the oligotrophic waters, picophytoplankton dominated (88–92%) TChl *a* inventories, while phytoplankton >3 μm comprised 8–12% of TChl *a* inventories. Despite these large differences in the size structure of phytoplankton assemblages between the upwelling-influenced and oligotrophic waters, the size partitioning of primary productivity appeared largely consistent across the transect. Larger (>2 μm) phytoplankton and picophytoplankton accounted for ~30–40% and ~60–70%, respectively, of the >0.2 μm ^{14}C-based productivity. Thus, while the contributions of different phytoplankton sizes to biomass and productivity are comparable to each other in the upwelling region, larger phytoplankton appeared, on a biomass-normalized basis, disproportionately active in oligotrophic waters. These observations, which imply that significant changes occur in photosynthetic activities of large phytoplankton without accompanying variations in biomass, have been observed in studies conducted in other ocean ecosystems (Malone 1980; Marañón et al. 2001; Li et al. 2011). Latasa et al. (2005), in a study that derived estimates of phytoplankton taxa-specific growth and grazing through measurements of pigment biomarkers, dilution experiments, and ^{14}C-based primary production, showed that specific taxa, such as diatoms, played a disproportionate role in carbon flux compared with their biomass due to their high growth and grazing rates. Similarly, it is likely that recycling of biomass must intensify in low

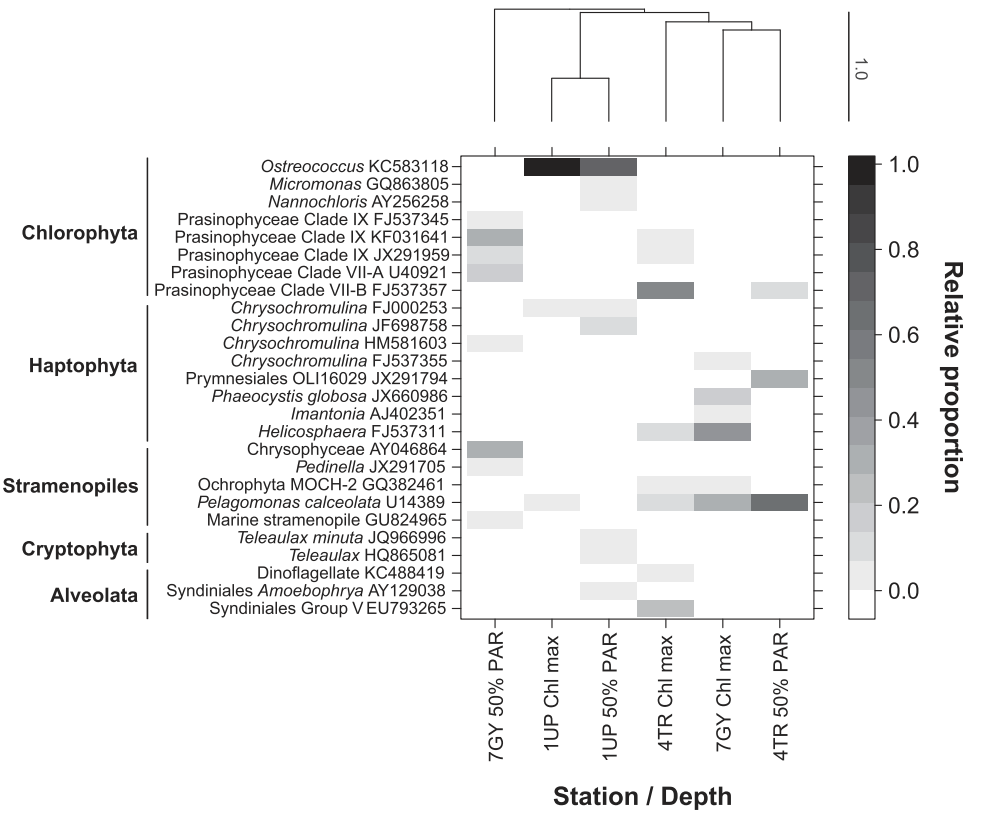

Fig. 4. Taxonomic composition of PPE assemblages based on 18S rRNA gene sequences obtained from flow cytometrically sorted cells from the 50% surface PAR isopleth and the Chl max at stations 1UP, 4TR, and 7GY. A total of 526 sequences were clustered at the 99% similarity threshold into OTUs by open reference picking with the SILVA 119 eukaryote database. The dendrogram, at height 1.0 being the most dissimilar, depicts clustering based on the Jaccard index.

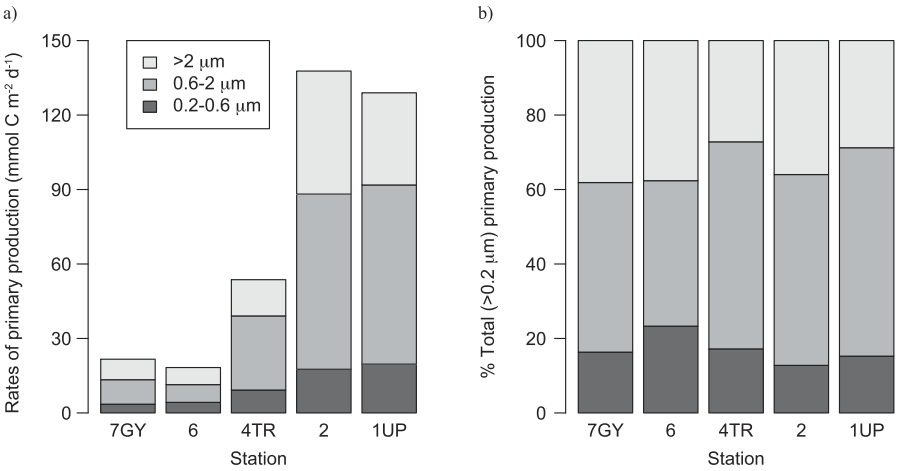

Fig. 5. (**a**) Euphotic zone depth-integrated (0.1% surface PAR for stations 1UP, 2, 4TR, and 6; depth of Chl max for St. 7GY) rates of ^{14}C-based primary production in three size fractions (>2 μm, 0.6–2 μm, and 0.2–0.6 μm) at station 1UP, 2, 4TR, 6, and 7GY. (**b**) Relative Contributions of size-fractionated rates to >0.2 μm ^{14}C-primary production.

nutrient waters to sustain productivity, with population sizes presumably under tight control by top-down processes such as microzooplankton grazing, viral lysis, and disease.

One of the striking observations made in our study was the consistent dominance of picophytoplankton as contributors to the measured rates of >0.2 μm ^{14}C-based productivity across

Table 4. Picophytoplankton ^{14}C-productivity and group- and cell-specific contributions.

	7GY	6	4TR	2
^{14}C-Primary production rates (mmol C m^{-2} d^{-1}), [% sum of sorts]*				
PPE	4.5 [48%]	4.6 [36%]	10.8 [44%]	23.6 [41%]
Prochlorococcus	4.3 [45%]	7.3 [57%]	11.6 [48%]	23.6 [41%]
Synechococcus	0.7 [7%]	0.8 [7%]	2.0 [8%]	10.6 [18%]
***Group contribution to CO_2 fixation (%)**†**				
PPE	21%	25%	20%	17%
Prochlorococcus	20%	40%	22%	17%
Synechococcus	3%	5%	4%	8%
Cell-specific primary production rates (fmol C cell^{-1} d^{-1})*				
PPE	28.6	16.3	32.8	34.9
Prochlorococcus	0.30	0.61	1.44	2.04
Synechococcus	9.40	11.8	7.69	5.32
Contribution to ^{14}C Primary production rates (%)*				
Sum of sorted cells/picoplankton productivity on filters	69	111	63	66
Sum of sorted cells/total (>0.2 μm) productivity on filters	43	70	46	42

*Rates and cellular stocks depth-integrated to the 0.1% surface PAR for St. 1UP-6 and to the Chl max for St. 7GY.
†Contributions are calculated as percent of >0.2 μm primary productivity captured on filters (see Fig. 5).

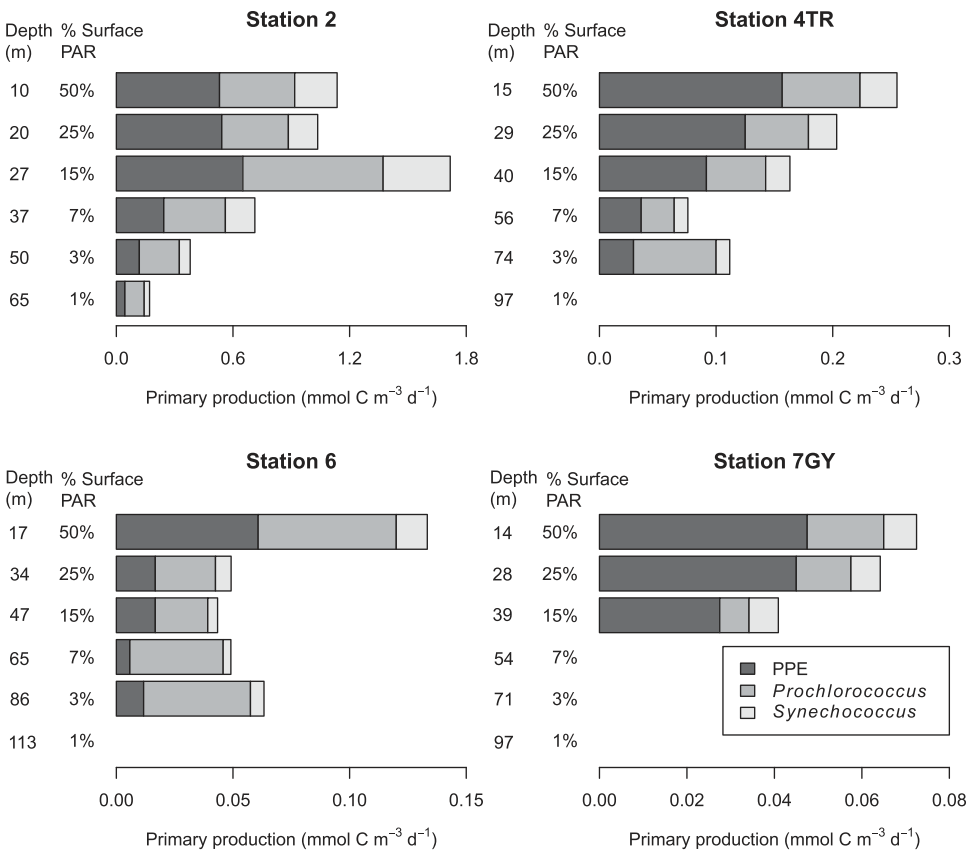

Fig. 6. Depth profiles of PPE, *Prochlorococcus*, and *Synechococcus* ^{14}C-based primary production rates at stations 2, 4TR, 6, and 7GY. Rates of primary production are binned by vertical isopleths (% surface PAR). Missing data indicate samples where there were too few cells to sort.

the biogeochemically diverse sampling regions. The observed increases in the biomass and productivity of larger phytoplankton in nutrient-enriched waters appear superimposed against a background of active picophytoplankton in these regions, a finding consistent with an active microbial food web across varying trophic states of the ocean (Margalef 1969; Yentsch and Phinney 1989; Chisholm 1992). Closer examination of picophytoplankton group-specific rates of ^{14}C-primary productivity provided further insight into productivity dynamics between PPE and cyanobacteria. Cellular abundances of *Prochlorococcus* were two orders of magnitude greater than PPE at all stations except at the upwelling station 1UP. Yet, cell-specific rates of productivity by *Prochlorococcus* were relatively low (ranging 0.3–2.0 fmol C cell^{-1} d^{-1}), while activities by PPE and *Synechococcus* were considerably greater (averaging 28 fmol C cell^{-1} d^{-1} and 9 fmol C cell^{-1} d^{-1}, respectively, Table 4). In fact, PPE cell-specific rates of productivity remained fairly consistent across the transect, while *Prochlorococcus* rates decreased into the SPSG; cell-specific PPE rates were 17-fold greater than *Prochlorococcus* at station 2, increasing to 93-fold greater at station 7GY (Table 4).

These results are consistent with the findings of Jardillier et al. (2010), who reported cell-specific PPE rates as much as 82-fold greater than those of *Prochlorococcus* in the subtropical and tropical northeast Atlantic Ocean. When taking into account their cell abundances, the proportional contributions by PPE and *Prochlorococcus* to rates of >0.2 μm ^{14}C-primary production were equivalent, with each group responsible for ~17–22% of the productivity at the main process stations in the study region (Table 4). This observation of their equal contributions to rates of >0.2 μm ^{14}C-primary productivity in biogeochemically distinct regions of the study region reveals that the partitioning of their photosynthetic activities remains surprisingly consistent despite large changes in cell biomass. However, the derived contributions to rates of ^{14}C-based primary productivity by these two groups of picophytoplankton varied with depth, with PPE appearing more active in the upper ocean and *Prochlorococcus* becoming increasingly important in the dimly-lit waters.

The important role of PPE in carbon cycling in the upper open ocean likely derives from the larger cell biovolumes of these cells relative to unicellular cyanobacteria (Zubkov et al. 2000; Worden et al. 2004; Jardillier et al. 2010). Similar to our results, Grob et al. (2011) concluded that cell-specific carbon uptake rates by PPE varied as a function of cell size, following the rule of isometric scaling of production (Marañón et al. 2007). While our estimates of PPE cell-specific rates of ^{14}C-productivity were on average 25-fold greater than those of *Prochlorococcus*, the biomass-normalized rates of productivity (using biovolume carbon conversion factors from Worden et al. 2004) were at least twofold greater among PPE (0.68 d^{-1}) than *Prochlorococcus* (0.35 d^{-1}) throughout the euphotic zones in the regions sampled for this study. These derived growth rates are highly dependent on volume-specific carbon conversion factors and equations used for biovolume and carbon content calculations, particularly for PPE, which can differ greatly in cell size. However, our rates are comparable to those reported in previous studies using varying techniques (Li 1994; Worden et al. 2004; Jardillier et al. 2010).

Similar to phytoplankton >3 μm in the oligotrophic SPSG, PPE were observed to have high growth rates without proportional biomass accumulation in each of the regions studied, implying that PPE assemblages are closely regulated by an analogous mortality rate. In a study examining growth and grazing mortality rates of picophytoplankton groups, Worden et al. (2004) found that a significant fraction of the net carbon produced was consumed immediately (e.g., more than 2.5 times the carbon equivalent to the visible PPE standing stock was produced and consumed without changes in standing stock measurements). Thus, despite the lower numerical abundance of PPE in various regions of the world's ocean, PPE appear to actively transfer carbon to higher trophic levels. Furthermore, picophytoplankton removal from the upper ocean may be a result of viral lysis and other causes of mortality (Baudoux et al. 2008; Bidle and Vardi 2011) as well as accelerated sinking through particle aggregation and mesozooplankton grazing, contributing to carbon export at rates proportional to their rates of production (Richardson and Jackson 2007).

We combined a suite of approaches to identify key PPE taxa observed to be responsible for this relatively large fraction of picophytoplankton production in the near-surface waters of the SEP. The PPE assemblage structure observed in this study is similar to previous reports of PPE assemblages found in upwelling regions of the SEP (Lepère et al. 2009; Shi et al. 2009; Kirkham et al. 2013). In the near-surface waters of station 1UP, pigments retrieved in the picophytoplankton size fraction included those diagnostic of prymnesiophytes, prasinophytes, and cryptophytes. The 18S rRNA gene sequence analyses revealed more taxa-specific results, with *Ostreococcus* (Mamiellophyceae) appearing as the dominant member of the PPE assemblage at station 1UP among other chlorophytes (*Micromonas* and *Nannochloris*), haptophytes (*Chrysochromulina*), and cryptophytes (*Teleaulax*). The sequences clustering among *Ostreococcus* appeared closely related to the "low-light" ecotype Clade OII (RCC393 and 143), and our results are consistent with known biogeographical distributions of these organisms (Demir-Hilton et al. 2011; Acosta et al. 2013). Clade OII have been previously described occurring in the deep chlorophyll maximum of warm (22 ± 3°C) oligotrophic waters and in the surface waters during periods of euphotic zone mixing, suggesting nutrient availability to be a determinant of OII vertical distribution in addition to light (Demir-Hilton et al. 2011). Quantitative PCR amplification of different clades of *Ostreococcus* indicates a cosmopolitan distribution of clade OII in offshore waters, including the relatively nutrient-enriched

waters of the Gulf Stream (Demir-Hilton et al. 2011). Similarly, in the current study, these *Ostreococcus* sequences were dominant in the nutrient-enriched waters of station 1UP where water temperatures remained relatively warm (~19°C).

In the oligotrophic waters of the SPSG, the combined use of pigment biomarkers and 18S rRNA gene sequences revealed that the near-surface PPE assemblages consisted of prasinophytes Clades VII and IX, diverse groups of stramenopiles such as Ochrophyta MOCH-2 and *Pelagomonas calceolata*, uncultivated marine chrysophytes, and various haptophytes including *Helicosphaera*, *Imantonia*, *Phaeocystis globosa*, and several uncultured *Chrysochromulina*. Many of these organisms have also been previously reported from similar oceanic habitats, including the SEP (Lepère et al. 2009; Shi et al. 2009; Kirkham et al. 2013). While taxa such as *Chrysochromulina* appeared to be ubiquitous along the transect, other taxa were region-specific, presumably reflecting taxon-specific balance between growth and removal. In particular, the biogeographic partitioning of different clades of Prasinophyceae suggests differing adaptations to bottom-up and top-down processes (e.g., nutrient acquisition, light availability, and mortality) among the Prasinophyceae class.

The relatively large proportion of sequences clustering among pico-haptophytes in the current study (108 total sequences out of 526 total) is notable, given the known mixotrophic capabilities of these organisms, obtaining nutrition and energy through bacterivory and/or photosynthesis (Estep and MacIntyre 1989; Liu et al. 2009; Kirkham et al. 2013). In addition, sequences retrieved among the PPE in the present study were closely related to various groups of prymnesiophytes and stramenopiles (Dictyochophyceae and Chrysophyceae), taxa that have been reported to feed on *Prochlorococcus* and *Synechococcus* (Frias-Lopez et al. 2009). It has been hypothesized that mixotrophs display such behavior to increase their relative fitness by reducing competitors in low-nutrient environments (Acosta et al. 2013). The prevalence of potentially mixotrophic taxa in the more oligotrophic waters of the study region may be indicative of a switch in metabolism among the PPE from photoautotrophy to mixotrophy along the gradient from high to low nutrient concentrations. If this is true, the amount of ^{14}C measured in mixotrophic cells retrieved from a ^{14}C-labeled incubation experiment may be slightly greater not only as a result of the assimilation of ^{14}C via autotrophy but also of the consumption of ^{14}C-labeled organic matter (e.g., other autotrophic cells). We expect the contribution of this "consumed" ^{14}C to be relatively small in magnitude, given the low cell-specific rates of carbon assimilation of cyanobacteria observed in this study and reported by others (Li 1994; Jardillier et al. 2010). However, if PPE are rapidly consuming cyanobacterial biomass, as suggested by Zubkov and Tarran (2008) and Hartmann et al. (2012), quantifying the contributions of photosynthetic and heterotrophic ^{14}C assimilation by these organisms may be an important consideration for future experiments.

From the Chl max at the transition station 4TR and from the near-surface at station 1UP, we retrieved sequences clustering among the Syndiniales (*Amoebophrya* and Group V), a parasitic group of alveolates. These organisms have been frequently retrieved from 18S rRNA gene sequencing analyses in marine ecosystems (with groups II, III, and V largely found in the photic zone) and hypothesized to be important generalist parasites (Massana et al. 2004; Guillou et al. 2008; Acosta et al. 2013). Our finding of these sequences from flow-sorted PPE populations was somewhat surprising, but may reflect the presence of parasites carried by the PPE cells themselves, or the simultaneous sorting of an undetected non-photosynthetic cell alongside a photosynthetic organism (Shi et al. 2009). Furthermore, it is possible that members of the Syndiniales retained ancestral traits such as photosynthetic capabilities, pigmentation, and/or phagotrophy (Guillou et al. 2008).

There are several potentially important methodological considerations that emerged from our measurements. First, the flow-sorting methodology may underestimate picophytoplankton production, as evidenced by the collective (flow-sorted PPE, *Prochlorococcus*, and *Synechococcus* cells) carbon fixation rates accounting for 63–111% of the productivity measured in the picoplanktonic fraction (0.2–2 μm) on filters. This underestimation is possibly due to low cell abundances of certain PPE taxa, resulting in the under-representation of rarer organisms, or due to cell breakage of fragile taxa occurring as a result of the preservation process. Second, for the 18S rRNA gene analyses, we sorted PPE cells that had been concentrated after excluding organisms >3 μm. However, for the filtration-based estimates of ^{14}C-productivity, picoplankton activity was quantified based on organisms <2 μm. Hence, if there were PPE with cell diameters in the 2–3 μm size range, they would have been included in the production rate measurements for the >2 μm fraction, thereby potentially underestimating the measured contributions by PPE to the 0.2–2 μm filter fraction. Finally, an additional source of methodological uncertainty in this study lies with the flow cytometric sorting of specific populations for phylogenetic information. It is possible that losses of more fragile PPE cells could have occurred as a result of the tangential flow filtration process, although samples were processed as quickly as possible (within 4–6 h of collection) at gentle flow rates. In an attempt to collect as many cells as possible for low abundance populations such as PPE, a delicate balance must be sought to maintain sample integrity while collecting a sufficient amount of material for subsequent analyses.

In summary, our study confirms that picophytoplankton are significant contributors to biomass and primary production in distinct biogeochemical regions of the South East Pacific Ocean. We found that despite cellular abundances that are lower by orders of magnitude, PPE contributed a nearly equivalent proportion to measured ^{14}C-primary productivity as the numerically dominant *Prochlorococcus*, a

finding consistent with the presumed larger cell-carbon content of the PPE. Moreover, we found that in the well-lit upper regions (>15% surface PAR) of the SPSG, rates of ^{14}C-productivity by PPE exceeded productivity by cyanobacteria. Cyanobacteria have long been thought to be the dominant picophytoplankton, numerically due to their high abundance as well as functionally due to their affinity for utilizing low concentrations of nutrients; yet, unique characteristics of prominent PPE taxa (haptophytes, cryptophytes, prasinophytes, and stramenopiles), such as their slightly larger size and reportedly mixotrophic metabolism, may allow them to thrive across the biogeochemically distinct regions sampled as part of this study. Moreover, the apparently high growth rates of PPE observed in the current study, without concomitant accumulation of biomass, suggests these organisms are rapidly removed via top-down processes and/or sinking. Combined, our study highlights the multifaceted ecology of PPE in different regions of the world's oceans, and provides new insight into the important role of these organisms in ocean carbon cycling.

References

Acker, J. G., and G. Leptoukh. 2007. Online analysis enhances use of NASA earth science data. EOS Trans. AGU **88**: 14–17. doi:10.1029/2007EO020003

Acosta, F., D. K. Ngugi, and U. Stingl. 2013. Diversity of picoeukaryotes at an oligotrophic site off the Northeastern Red Sea Coast. Aquat. Biosyst. **9**: 16. doi:10.1186/2046-9063-9-16

Andersen, R. A., G. W. Saunders, M. P. Paskind, and J. P. Sexton. 1993. Ultrastructure and 18S rRNA gene sequence for *Pelagomonas calceolata* gen. et. sp. nov. and the description of a new algal class, the *Pelagophyceae classis* nov. J. Phycol. **29**: 701–715. doi:10.1111/j.0022-3646.1993.00701.x

Armstrong, F. A. J., C. R. Stearns, and J. D. H. Strickland. 1967. The measurement of upwelling and subsequent biological processes by means of the Technicon AutoAnalyzer™ and associated equipment. Deep-Sea Res. **14**: 381–389. doi:10.1016/0011-7471(67)90082-4

Baldauf, S. 2003. The deep roots of eukaryotes. Science **300**: 1703–1706. doi:10.1126/science.1085544

Balzano, S., D. Marie, P. Gourvil, and D. Vaulot. 2012. Composition of the summer photosynthetic pico and nanoplankton communities in the Beaufort Sea assessed by T-RFLP and sequences of the 18S rRNA gene from flow cytometry sorted samples. ISME J. **6**: 1480–1498. doi:10.1038/ismej.2011.213

Baudoux, A. C., M. Veldhuis, A. Noordeloos, G. Van Noort, and C. Brussaard. 2008. Estimates of virus- vs. grazing induced mortality of picophytoplankton in the North Sea during summer. Aquat. Microb. Ecol. **52**: 69–82. doi:10.3354/ame01207

Bidigare, R. R., L. Van Heukelem, and C. C. Trees. 2005. Analysis of algal pigments by high-performance liquid chromatography, p. 327–345. *In* R. A. Anderson [ed.], Algal culturing techniques. Academic Press.

Bidle, K. D., and A. Vardi. 2011. A chemical arms race at sea mediates algal host–virus interactions. Curr. Opin. Microb. **14**: 449–457. doi:10.1016/j.mib.2011.07.013

Caporaso, J. G., and others. 2010. QIIME allows analysis of high-throughput community sequencing data. Nat. Methods **7**: 335–336. doi:10.1038/nmeth.f.303

Caron, D. A., A. Z. Worden, P. D. Countway, E. Demir, and K. B. Heidelberg. 2009. Protists are microbes too: A perspective. ISME J. **3**: 4–12. doi:10.1038/ismej.2008.101

Carr, M. E., and others. 2006. A comparison of global estimates of marine primary production from ocean color. Deep-Sea Res. II **53**: 741–770. doi:10.1016/j.dsr2.2006.01.028

Chisholm, S. W. 1992. Phytoplankton size, p. 213–237. *In* P. G. Falkowski and A. D. Woodhead [eds.], Primary productivity and biogeochemical cycles in the sea. Springer.

Cuvelier, M. L., and others. 2010. Targeted metagenomics and ecology of globally important uncultured eukaryotic phytoplankton. Proc. Natl. Acad. Sci. USA **107**: 14679–14684. doi:10.1073/pnas.1001665107

Decelle, J., and others. 2012. An original mode of symbiosis in open ocean plankton. Proc. Natl. Acad. Sci. USA **109**: 18000–18005. doi:10.1073/pnas.1212303109

Demir-Hilton, E., S. Sudek, M. L. Cuvelier, C. L. Gentemann, J. P. Zehr, and A. Z. Worden. 2011. Global distribution patterns of distinct clades ofthe photosynthetic picoeukaryote *Ostreococcus*. ISME J. **5**: 1095–1107. doi:10.1038/ismej.2010.209

Duhamel, S., F. Zeman, and T. Moutin. 2006. A dual-labeling method for the simultaneous measurement of dissolved inorganic carbon and phosphate uptake by marine planktonic species. Limnol. Oceanogr.: Methods **4**: 416–425. doi:10.4319/lom.2006.4.416

Duhamel, S., and T. Moutin. 2009. Carbon and phosphate incorporation rates of microbial assemblages in contrasting environments in the Southeast Pacific. Mar. Ecol. Prog. Ser. **375**: 53–64. doi:10.3354/meps07765

Edgar, R. C., B. J. Haas, J. C. Clemente, C. Quince, and R. Knight. 2011. UCHIME improves sensitivity and speed of chimera detection. Bioinformatics **27**: 2194–2200. doi:10.1093/bioinformatics/btr381

Edgcomb, V. P., D. T. Kysela, A. Teske, A. de Vera Gomez, and M. L. Sogin. 2002. Benthic eukaryotic diversity in the Guaymas Basin hydrothermal vent environment. Proc. Natl. Acad. Sci. USA **99**: 7658–7662. doi:10.1073/pnas.062186399

Edgcomb, V. P., and others. 2011. Protistan microbial observatory in the Cariaco Basin, Caribbean. I. Pyrosequencing vs Sanger insights into species richness. ISME J. **5**: 1344–1356. doi:10.1038/ismej.2011.6

Estep, K. W., and F. MacIntyre. 1989. Taxonomy, life cycle, distribution and dasmotrophy of *Chrysochromulina*: A theory accounting for scales, haptonema, muciferous

bodies and toxicity. Mar. Ecol. Prog. Ser. **57**: 11–21. doi:10.3354/meps057011

Field, C. B., M. J. Behrenfeld, J. T. Randerson, and P. G. Falkowski. 1998. Primary production of the biosphere: Integrating terrestrial and oceanic components. Science **281**: 237–240. doi:10.1126/science.281.5374.237

Frias-Lopez, J., A. Thompson, J. Waldbauer, and S. W. Chisholm. 2009. Use of stable isotope-labelled cells to identify active grazers of picocyanobacteria in ocean surface waters. Environ. Microbiol. **11**: 512–525. doi:10.1111/j.1462-2920.2008.01793.x

Fuller, N. J., and others. 2006. Analysis of photosynthetic picoeukaryote diversity at open ocean sites in the Arabian Sea using a PCR biased towards marine algal plastids. Aquat. Microb. Ecol. **43**: 79–93. doi:10.3354/ame043079

Gordon, L. I., J. C. Jennings, A. A. Ross, and J. M. Krest. 1994. A suggested protocol for continuous flow analysis of seawater nutrients (phosphate, nitrate, nitrite, and silicic acid) in the WOCE Hydrographic Program and Joint Global Ocean Fluxes Study. WHP Office Report 91-1.

Grob, C., M. Hartmann, M. V. Zubkov, and D. J. Scanlan. 2011. Invariable biomass-specific primary production of taxonomically discrete picoeukaryote groups across the Atlantic Ocean. Environ. Microbiol. **13**: 3266–3274. doi:10.1111/j.1462-2920.2011.02586.x

Guillou, L., and others. 2004. Diversity of picoplanktonic prasinophytes assessed by direct nuclear SSU rDNA sequencing of environmental samples and novel isolates retrieved from oceanic and coastal marine ecosystems. Protist **155**: 193–214. doi:10.1078/143446104774199592

Guillou, L., and others. 2008. Widespread occurrence and genetic diversity of marine parasitoids belonging to Syndiniales (Alveolata). Environ. Microbiol. **10**: 3349–3365. doi:10.1111/j.1462-2920.2008.01731.x

Hartmann, M., C. Grob, G. A. Tarran, A. P. Martin, P. H. Burkill, D. J. Scanlan, and M. V. Zubkov. 2012. Mixotrophic basis of Atlantic oligotrophic ecosystems. Proc. Natl. Acad. Sci. USA **109**: 5756–5760. doi:10.1073/pnas.1118179109

Jardillier, L., M. V. Zubkov, J. Pearman, and D. J. Scanlan. 2010. Significant CO_2 fixation by small prymnesiophytes in the subtropical and tropical northeast Atlantic Ocean. ISME J. **4**: 1180–1192. doi:10.1038/ismej.2010.36

Jeffrey, S. W., S. W. Wright, and M. Zapata. 2011. Microalgal classes and their signature pigments. p. 3–77. *In* S. Roy, A. Llewellyn, E. S. Egeland and G. Johnsen [eds.], Phytoplankton pigments: Characterization, chemotaxonomy, and applications in oceanography. Cambridge University Press.

Kirkham, A. R., L. E. Jardillier, A. Tiganescu, J. Pearman, M. V. Zubkov, and D. J. Scanlan. 2011. Basin-scale distribution patterns of photosynthetic picoeukaryotes along an Atlantic Meridional Transect. Environ. Microbiol. **13**: 975–990. doi:10.1111/j.1462-2920.2010.02403.x

Kirkham, A. R., C. Lepère, L. E. Jardillier, F. Not, H. Bouman, A. Mead, and D. J. Scanlan. 2013. A global perspective on marine photosynthetic picoeukaryote community structure. ISME J. **7**: 922–936. doi:10.1038/ismej.2012.166

Latasa, M., R. R. Bidigare, M. E. Ondrusek, and M. C. Kennicutt, II. 1996. HPLC analysis of algal pigments: A comparison exercise among laboratories and recommendations for improved analytical performance. Mar. Chem. **51**: 315–324. doi:10.1016/0304-4203(95)00056-9

Latasa, M., X. A. G. Morán, R. Scharek, and M. Estrada. 2005. Estimating the carbon flux through main phytoplankton groups in the northwestern Mediterranean. Limnol. Oceanogr. **50**: 1447–1458. doi:10.4319/lo.2005.50.5.1447

Laza-Martinez, A., J. Arluzea, I. Miguel, and E. Orive. 2012. Morphological and molecular characterization of *Teleaulax gracilis* sp. nov. and *T. minuta* sp. nov. (Cryptophyceae). Phycologia **51**: 649–661. doi:10.2216/11-044.1

Lepère, C., D. Vaulot, and D. J. Scanlan. 2009. Photosynthetic picoeukaryote community structure in the South East Pacific Ocean encompassing the most oligotrophic waters on earth. Environ. Microbiol. **11**: 3105–3117. doi:10.1111/j.1462-2920.2009.02015.x

Li, W. K. W. 1994. Primary production of prochlorophytes, cyanobacteria, and eukaryotic ultraphytoplankton: Measurements from flow cytometric sorting. Limnol. Oceanogr. **39**: 169–175. doi:10.4319/lo.1994.39.1.0169

Li, B., D. M. Karl, R. M. Letelier, and M. J. Church. 2011. Size-dependent photosynthetic variability in the North Pacific Subtropical Gyre. Mar. Ecol. Prog. Ser. **440**: 27–40. doi:10.3354/meps09345

Liu, H., and others. 2009. Extreme diversity in noncalcifying haptophytes explains a major pigment paradox in open oceans. Proc. Natl. Acad. Sci. USA **106**: 12803–12808. doi:10.1073/pnas.0905841106

Malone, T. C. 1980. Size-fractionated primary productivity of marine phytoplankton, p. 301–319. *In* P. G. Falkowski [ed.], Primary productivity in the sea. Plenum Press.

Marañón, E., P. Holligan, R. Barciela, N. González, B. Mouriño, M. Pazó, and M. Varela. 2001. Patterns of phytoplankton size structure and productivity in contrasting open-ocean environments. Mar. Ecol. Prog. Ser. **216**: 43–56. doi:10.3354/meps216043

Marañón, E., and others. 2007. Planktonic carbon budget in the eastern subtropical North Atlantic. Aquat. Microb. Ecol. **48**: 261–275. doi:10.3354/ame048261

Margalef, R. 1969. Size of centric diatoms as an ecological indicator. Mitt. Internat. Verein. Limnol. **17**: 202–210.

Massana, R. 2011. Eukaryotic picoplankton in surface oceans. Annu. Rev. Microbiol. **65**: 91–110. doi:10.1146/annurev-micro-090110-102903

Massana, R., V. Balagué, L. Guillou, and C. Pedrós-Alió. 2004. Picoeukaryotic diversity in an oligotrophic coastal site studied by molecular and culturing approaches. FEMS Microbiol. Ecol. **50**: 231–243. doi:10.1016/j.femsec.2004.07.001

Massana, R., J. del Campo, M. E. Sieracki, S. Audic, and R. Logares. 2014. Exploring the uncultured microeukaryote majority in

the oceans: Reevaluation of ribogroups within stramenopiles. ISME J. **8**: 854–866. doi:10.1038/ismej.2013.204

Moon-van der Staay, S. Y., G. W. M. van der Staay, L. Guillou, D. Vaulot, H. Claustre, and L. K. Medlin. 2000. Abundance and diversity of prymnesiophytes in the picoplankton community from the equatorial Pacific Ocean inferred from 18S rDNA sequences. Limnol. Oceanogr. **45**: 98–109. doi:10.4319/lo.2000.45.1.0098

Moutin, T., P. Raimbault, and J. C. Poggiale. 1999. Primary production in surface waters of the western Mediterranean sea. Calculation of daily production. C.R. Acad. Sci. III-Vie. **322**: 651–659. doi:10.1016/S0764-4469(99)80104-8

Oksanen, J., and others. 2013. Package 'vegan': Community ecology package. R package version 2.0-10. Available from http://cran.r-project.org/web/packages/vegan/.

Orsi, W., Y. C. Song, S. Hallam, and V. Edgcomb. 2012. Effect of oxygen minimum zone formation on communities of marine protists. ISME J. **6**: 1586–1601. doi:10.1038/ismej.2012.7

Potter, D., T. C. LaJeunesse, G. W. Saunders, and R. A. Anderson. 1997. Convergent evolution masks extensive biodiversity among marine coccoid picoplankton. Biodivers. Conserv. **6**: 99–107. doi:10.1023/A:1018379716868

Quast, C., and others. 2013. The SILVA ribosomal RNA gene database project: Improved data processing and web-based tools. Nucl. Acids Res. **41**: D590–D596. doi:10.1093/nar/gks1219

Richardson, T. L., and G. A. Jackson. 2007. Small phytoplankton and carbon export from the surface ocean. Science **315**: 838–840. doi:10.1126/science.1133471

Romari, K., and D. Vaulot. 2004. Composition and temporal variability of picoeukaryote communities at a coastal site of the English Channel from 18S rDNA sequences. Limnol. Oceanogr. **49**: 784–798. doi:10.4319/lo.2004.49.3.0784

Shi, X. L., D. Marie, L. Jardillier, D. J. Scanlan, and D. Vaulot. 2009. Groups without cultured representatives dominate eukaryotic picophytoplankton in the oligotrophic South East Pacific Ocean. PLoS ONE **4**: e7657. doi:10.1371/journal.pone.0007657

Sieburth, J. M., V. Smetacek, and J. Lenz. 1978. Pelagic ecosystem structure: Heterotrophic compartments of the plankton and their relationship to plankton size fractions. Limnol. Oceanogr. **23**: 1256–1263. doi:10.4319/lo.1978.23.6.1256

Steemann Nielsen, E. 1952. The use of radioactive carbon (^{14}C) for measuring organic production in the sea. J. Conseil. **18**: 117–140. doi:10.1093/icesjms/18.2.117

Stoeck, T., G. T. Taylor, and S. S. Epstein. 2003. Novel eukaryotes from the permanently anoxic Cariaco Basin (Caribbean Sea). Appl. Environ. Microbiol. **69**: 5656–5663. doi:10.1128/AEM.69.9.5656-5663.2003

Thompson, J. D., D. G. Higgins, and T. J. Gibson. 1994. CLUSTAL W: Improving the sensitivity of progressive multiple sequence alignment through sequence weighting, position-specific gap penalties and weight matrix choice. Nucl. Acids Res. **22**: 4673–4680. doi:10.1093/nar/22.22.4673

Thompson, A. W., and others. 2012. Unicellular cyanobacterium symbiotic with a single-celled eukaryotic alga. Science **337**: 1546–1550. doi:10.1126/science.1222700

Vaulot, D., W. Eikrem, and M. Viprey. 2008. The diversity of small eukaryotic phytoplankton (≤ 3 μm) in marine ecosystems. FEMS Microbiol. Rev. **32**: 795–820. doi:10.1111/j.1574-6976.2008.00121.x

Worden, A. Z. 2006. Picoeukaryote diversity in coastal waters of the Pacific Ocean. Aquat. Microb. Ecol. **43**: 165–175. doi:10.3354/ame043165

Worden, A. Z., J. K. Nolan, and B. Palenik. 2004. Assessing the dynamics and ecology of marine picophytoplankton: The importance of the eukaryotic component. Limnol. Oceanogr. **49**: 168–179. doi:10.4319/lo.2004.49.1.0168

Wu, W., B. Huang, and C. Zhong. 2014. Photosynthetic picoeukaryote assemblages in the South China Sea from the Pearl River estuary to the SEATS station. Aquat. Microb. Ecol. **71**: 271–284. doi:10.3354/ame01681

Yentsch, C. S., and D. A. Phinney. 1989. A bridge between ocean optics and microbial ecology. Limnol. Oceanogr. **34**: 1694–1705. doi:10.4319/lo.1989.34.8.1694

Zubkov, M. V., M. A. Sligh, P. H. Burkill, and R. J. G. Leakey. 2000. Picoplankton community structure on the Atlantic Meridional Transect: A comparison between seasons. Prog. Oceanogr. **45**: 369–386. doi:10.1016/S0079-6611(00)00008-2

Zubkov, M. V., and G. A. Tarran. 2008. High bacterivory by the smallest phytoplankton in the North Atlantic Ocean. Nature **455**: 224–226. doi:10.1038/nature07236

Acknowledgments

The authors would like to thank the captain and crew of R/V *Melville* and the participants of the BiG RAPA expedition for assistance with data collection for this project. We also acknowledge Ken Doggett, Brandon Carter, Anne Thompson, and Karin Björkman for help with cell sorting, Mariona Segura-Noguera for measurements of dissolved inorganic carbon used in calculations of primary production, and Joe Jennings for macronutrient analyses. Support for this work derived from U.S. National Science Foundation grants to C-MORE (EF-0424599; DMK) and OCE-1241263 (MJC). Additional support was received from the University of Hawai'i Denise B. Evans Research Fellowship in Oceanography (YMR), the Gordon and Betty Moore Foundation (DMK), and the Simons Foundation via the Simons Collaboration on Ocean Processes and Ecology (SCOPE: DJR, MJC, and DMK).

Submitted 21 May 2015
Revised 5 September 2015
Accepted 30 November 2015

Associate editor: Mikhail Zubkov